Audio Engineering Society

Convention Paper 9098

Presented at the 137th Convention
2014 October 9–12 Los Angeles, USA

This Convention paper was selected based on a submitted abstract and 750-word precis that have been peer reviewed by at least two qualified anonymous reviewers. The complete manuscript was not peer reviewed. This convention paper has been reproduced from the author's advance manuscript without editing, corrections, or consideration by the Review Board. The AES takes no responsibility for the contents. Additional papers may be obtained by sending request and remittance to Audio Engineering Society, 60 East 42nd Street, New York, New York 10165-2520, USA; also see www.aes.org. All rights reserved. Reproduction of this paper, or any portion thereof, is not permitted without direct permission from the Journal of the Audio Engineering Society.

On Spatial-Aliasing-Free Sound Field Reproduction using Finite Length Line Source Arrays

Frank Schultz, Till Rettberg and Sascha Spors

Institute of Communications Engineering, University of Rostock, Germany

Correspondence should be addressed to Frank Schultz (frank.schultz@uni-rostock.de)

ABSTRACT

Concert sound reinforcement systems aim at the reproduction of homogeneous sound fields over extended audiences for the whole audio bandwidth. For the last two decades this has been mostly approached by using so called line source arrays for which Wavefront Sculpture Technology (WST) was introduced in the literature. This paper utilizes a signal processing model developed for sound field synthesis in order to analyze and expand WST criteria for straight arrays. Starting with the driving function for an infinite and continuous linear array, spatial truncation and discretization are subsequently taken into account. The role of the involved loudspeakers as a spatial lowpass filter is stressed, which can reduce undesired spatial aliasing contributions. The paper aims to give a better insight on how to interpret the synthesized sound fields.

1. INTRODUCTION

In [1] we introduced a framework using sound field synthesis (SFS) and spatial sampling theory to revisit infinite Line Source Arrays (LSA) using Wavefront Sculpture Technology[1] (WST) [2, 3]. The SFS theory has been extensively used in the context of Wave Field Synthesis (WFS) research [4–14] and is strongly linked to aperture theory in Fourier acoustics/optics [15–17] and antenna design [18, 19].

So-called 2.5-dimensional SFS [6, Ch. 3] aims at the synthesis of a virtual source within a horizontal listening plane by a horizontally located loudspeaker array, often termed secondary source distribution (SSD). The listening area and loudspeaker array are typically of about the same size, as for many practically built WFS setups. In [20] it was

[1] Wavefront Sculpture Technology® is a registered trademark of L-ACOUSTICS US, LLC. We omit the labeling in the remainder of the paper and will only use the relevant research results.

discussed that synthesizing a virtual source is only possible within the so-called Fresnel region [19, Ch. 2.2.4] of the SSD.

Sound reinforcement using LSAs has been traditionally seen as radiation synthesis using electronic and/or geometric beamforming and -steering methods. Vertical loudspeaker arrays are commonly used in a linear, curved, spiral, arc or J-shaped arrangement [21]. In contrast to typical SFS setups, the listening area is usually much larger than the employed loudspeaker arrays. An optimum radiation has to be found that ensures a smooth frequency response over the whole audience area and frequency independent, homogeneous amplitude loss per distance doubling. Additional constraints such as quiet zones may also be imposed. It is well known that beam shaping is only possible for a wave length that is smaller than the length of the LSA. Hence the Fresnel region of an LSA has to be optimized for a homogeneous sound field [2, 3].

Although SFS and radiation synthesis aim at different target areas, the same analytical treatment can be performed. Therefore recent results of SFS research may be applied to LSA applications, which constitutes the main motivation for the presented work. In [6, Ch. 5] WFS reproduction of a virtual spherical monopole was analyzed with an acoustic signal processing framework. In [1] we argued that sound reinforcement with LSAs can be modeled as a special case of SFS: the synthesis of a cylindrical wave perpendicular to the array that is uniformly driven. The problem formulation starts with a linear, continuous and infinite SSD. Spatial discretization is subsequently modeled by spatially sampling the driving function. The individual sources can be represented by baffled piston models. Assuming identical characteristics for each secondary source, the sampling process can be formulated in the corresponding angular spectrum domain, where spectral repetitions are introduced. We conclude that the loudspeaker directivity acts as a spatial lowpass filter, i.e. the reconstruction filter within the sampling model. Ideally, the spatial lowpass has to suppress the spectral repetitions of the sampled driving function for perfect reconstruction of the sound field. If the suppression is imperfect the Green's function's angular spectrum (i.e. the spatially not bandlimited spectrum of a spherical monopole) is triggered by the spectral repetitions and undesired waves corrupt the intended sound field. This is known as reconstruction error or post-aliasing. In [9, Ch. 3.3,3.4] different loudspeakers and thereby postfilters were discussed in the context of WFS.

We further have shown that a spatial-aliasing-free sound field for the discussed special case can only be realized either by choosing the sampling distance smaller then the radiated wave length λ, cf. [1, (23)], or by using line pistons with the same length as the sampling interval, cf. [1, (38,39)]. For all other cases spatial aliasing will occur by either employing circular or line pistons. The tolerated amount of spatial aliasing energy and hence the quality of the produced sound field is a critical design criterion of LSAs. In [2, 3] the usage of waveguides for high audio frequencies was motivated and the 1st WST criterion defines an active radiation factor (ARF) as the quotient of piston length and sampling distance. For ARF ≥ 0.82, spatial aliasing contributions are at least 13.5 dB lower than that of the desired wave. This criterion was initially derived for finite length LSAs modeled with line pistons.

In this paper we will extend the signal processing framework towards finite length, linear LSAs. The finite array is modeled by spatially windowing the driving function. The advantage of the proposed viewpoint is the strict separation of spatial truncation, spatial sampling and pre-/postfiltering that might lead to better insights of the phenomena, cf. [6].

In Sec. 3 we summarize the outcome of [1], the model for an infinite, discrete SSD. Sec. 4 introduces the finite length, continuous line array. In Sec. 5 both models are combined, discussing finite length arrays modeled with discrete sources. Finally, a discussion on electronic beamsteering follows in Sec. 6.

2. NOMENCLATURE

A position vector in space is given by

$$\mathbf{x} = \begin{pmatrix} x \\ y \\ z \end{pmatrix} = \|\mathbf{x}\| \cdot \begin{pmatrix} \cos\varphi & \sin\vartheta \\ \sin\varphi & \sin\vartheta \\ & \cos\vartheta \end{pmatrix} \tag{1}$$

with azimuth $\varphi \in [0, 2\,\pi)$, colatitude $\vartheta \in [0, \pi]$ and the vector norm $\|\mathbf{x}\| = r = \sqrt{x^2 + y^2 + z^2}$. The SSD with finite length L and the spatial discretization Δy is located on the y-axis, for which we later choose an odd number of individual sources N at

$|y| \leq L/2$. The sound field is evaluated in the xy-plane for $x > 0$, cf. Fig. 1. The dispersion relation of linear acoustics

$$(\frac{\omega}{c})^2 = k_x^2 + k_y^2 + k_z^2 \tag{2}$$

holds. A constant speed of sound c=343 m/s, free-field conditions and a dissipationless medium are assumed. The wave number k_y describes the wave propagation along the SSD. For a cylindrical wave (CW) the radial wave number k_r is defined by

$$(\frac{\omega}{c})^2 - k_y^2 = \underbrace{(\frac{\omega}{c})^2 \left(\cos^2\varphi_{\mathrm{CW}} \sin^2\vartheta_{\mathrm{CW}} + \cos^2\vartheta_{\mathrm{CW}}\right)}_{k_r^2 = k_x^2 + k_z^2} \tag{3}$$

for our 2.5D scenario. We are only interested in the sound field within the xy-plane (i.e. $z = 0, \vartheta = \pi/2$), so the axial and radial wave numbers simplify to

$$k_y = \frac{\omega}{c} \sin\varphi_{\mathrm{CW}}\,, \qquad k_r = \frac{\omega}{c} \cos\varphi_{\mathrm{CW}}\,. \tag{4}$$

The main part of this paper treats the special case of wave propagation perpendicular to the SSD into

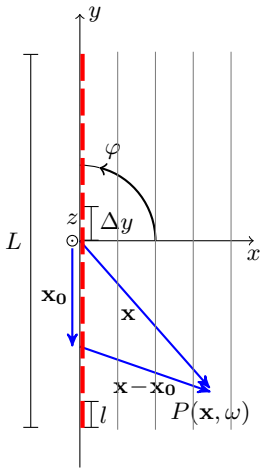

Fig. 1: Side view of the discussed, schematic SSD setup with length L using $N = 11$ line pistons of length l on the y-axis. The distance between the centers of two adjacent pistons is indicated as the spatial discretization step Δy. Sound field reproduction is considered within the xy-plane for $x > 0$. Wave propagation angle is indicated with φ.

direction of positive x. This corresponds to a radiation angle $\varphi_{\mathrm{CW}} = 0°$ or $k_y = 0\,\mathrm{rad/m}$ and $k_r = \frac{\omega}{c}$, respectively. For this case, we recall the required driving function's angular spectrum for the continuous, infinite SSD [1, (16)]

$$D(k_y, \omega) = 2\,\pi\,\delta(k_y) \cdot 2\,\pi\,\delta(\omega - \omega_{\mathrm{CW}}) \tag{5}$$

and the equidistantly sampled driving function's angular spectrum with $\Delta k_y = 2\,\pi/\Delta y$ [1, (21)]

$$D_{\mathrm{S}}(k_y, \omega) = \left(\frac{2\,\pi}{\Delta y} \sum_{\mu=-\infty}^{+\infty} \delta(k_y - \mu\,\frac{2\,\pi}{\Delta y})\right) \times 2\,\pi\,\delta(\omega - \omega_{\mathrm{CW}}). \tag{6}$$

We use the farfield directivities of rigid baffled pistons that are located within the yz-plane. These can be interpreted as postfilters $H_{\mathrm{Post}}(k_x, \omega)$, acting on the sampled driving function. For a circular piston with radius r_0 ($r_0^2 = y_0^2 + z_0^2$) the postfilter is given as [22, (26.42)], [23, (7.4.17)], [1, (32)]

$$H_{\mathrm{Circ}}(k_y, \omega) = \frac{2\,J_1(k_y\,r_0)}{k_y\,r_0} = \frac{2\,J_1(\frac{\omega}{c}\,\sin\varphi\,r_0)}{\frac{\omega}{c}\,\sin\varphi\,r_0}, \tag{7}$$

where $J_1(\cdot)$ denotes the cylindrical Bessel function of 1st kind of 1st order [24, (10.2.2)]. Note that for negative k_y [24, (10.11.1)] is valid. The line piston of length l along the y-axis and infinitesimal width centered at the origin is characterized by the unit amplitude normalized postfilter [22, (26.44)], [23, (7.3.3)], [1, (33)]

$$H_{\mathrm{Rect}}(k_y, \omega) = \frac{\sin\left(k_y\,\frac{l}{2}\right)}{k_y\,\frac{l}{2}} = \frac{\sin\left(\frac{\omega}{c}\,\sin\varphi\,\frac{l}{2}\right)}{\frac{\omega}{c}\,\sin\varphi\,\frac{l}{2}}. \tag{8}$$

In Fig. 2 the angular spectra $|H_{\mathrm{post}}(k_y, \omega)|$ of a 3" circular and line piston are exemplarily given.

In the half plane of interest with $x > 0$ and $z = 0$ the angular spectrum of the Green's function is given as [11, (52)]

$$G_0(x, k_y, \omega) = -\frac{\mathrm{j}}{4}\,H_0^{(2)}(\sqrt{(\frac{\omega}{c})^2 - k_y^2} \cdot x) \tag{9}$$

for propagating waves, i.e. $|k_y| < \frac{\omega}{c}$. $H_0^{(2)}(\cdot)$ denotes the 0th order cylindrical Hankel function of 2nd kind [24, §10.1]. Throughout the calculus, evanescent waves are not considered since the postfilter

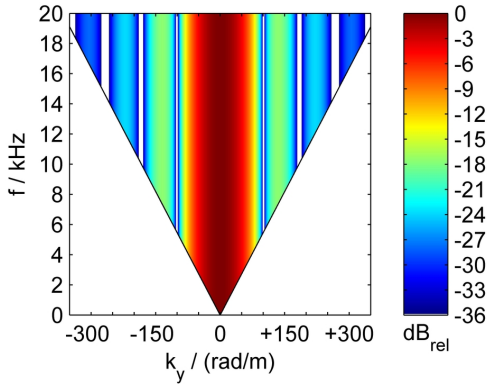

(a) Postfilter $|H_{\mathrm{Circ}}(k_y, \omega)|$ in dB according to (7) for a circular piston with diameter $2\,r_0 = 3$".

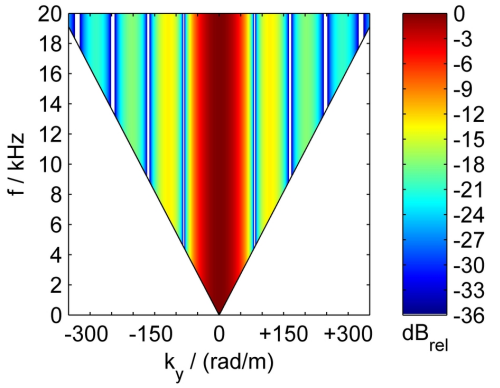

(b) Postfilter $|H_{\mathrm{Rect}}(k_y, \omega)|$ in dB according to (8) for a line piston with length $l = 3$".

Fig. 2: Angular spectra of a baffled circular and a baffled line piston.

models hold only under farfield assumptions. As a formal consequence, we define $H_{\mathrm{Post}}(k_y, \omega) = 0$ for $|k_y| > \frac{\omega}{c}$ and likewise $G_0(x, k_y, \omega)$. Similarly, an inverse spatial Fourier transform of the propagating contributions of a spectrum $P(x, k_y, \omega)$ is given by

$$\mathcal{F}^{-1}_{|k_y| \leq \frac{\omega}{c}} \{P(x, k_y, \omega)\} := \frac{1}{2\,\pi} \int_{-\frac{\omega}{c}}^{+\frac{\omega}{c}} P(x, k_y, \omega)\, \mathrm{e}^{-\mathrm{j}\, k_y\, y}\, \mathrm{d}k_y. \tag{10}$$

The temporal inverse Fourier transform

$$\mathcal{F}^{-1}_{\omega} \{P(x, k_y, \omega)\} := \frac{1}{2\,\pi} \int_{-\infty}^{+\infty} P(x, k_y, \omega)\, \mathrm{e}^{+\mathrm{j}\,\omega\, t}\, \mathrm{d}\omega \tag{11}$$

is used.

Note that the uniformly driven circular piston model is only valid for $\lambda \ll r_0$ for real loudspeakers. Furthermore the assumption of an infinite baffle is violated in practice for circular / line pistons and the LSA. For high frequencies the modeling is nonetheless useful and allows direct comparison with [2].

3. INFINITE, DISCRETIZED LSA

This section summarizes the outcome of [1] together with the analytical treatment of [11, Sec. IV.B]. The angular spectrum of the synthesized sound field using an infinite, discretized, uniformly driven, linear array modeled with pistons (7),(8) is with (6),(9) given as [1, (24)]

$$P(x, k_y, \omega) = \overbrace{D_{\mathrm{S}}(k_y, \omega) \cdot \underbrace{H_{\mathrm{Post}}(k_y, \omega)}_{\text{loudspeaker as spatial lowpass}}}^{\text{sampling \& reconstruction}} \cdot\, G_0(x, k_y, \omega) \tag{12}$$

for the considered xy-half-plane. A constant postfilter $H_{\mathrm{Post}}(k_y, \omega) = 1$ corresponds to reproduction with spherical monopoles and the sound field is analytically given as [11, (37)]

$$P(x, y, \omega) = \frac{1}{\Delta y}\, 2\,\pi\, \delta(\omega - \omega_{\mathrm{CW}}) \times \sum_{\mu=-\infty}^{+\infty} G_0(x, k_y = \mu\, \frac{2\,\pi}{\Delta y}, \omega) \cdot \mathrm{e}^{-\mathrm{j}\,\mu\, \frac{2\,\pi}{\Delta y}\, y}, \tag{13}$$

by inverse spatial Fourier transform and subsequent simplification. For $|\mu\, \Delta k_y| < \frac{\omega}{c}$ only propagating waves are taken into account, which reduces the sum in (13) to finite extent. The exponential term in (13) describes the component along the y-dimension. Note the discrete set of possible wave numbers due to the discrete driving function's angular spectrum. The Green's function's angular spectrum describes the component into radial direction. Both components together describe a cylindrical wave with radiation angle φ_μ. For $\mu = 0$ the intended cylindrical wave perpendicular to the SSD (i.e. into x-direction)

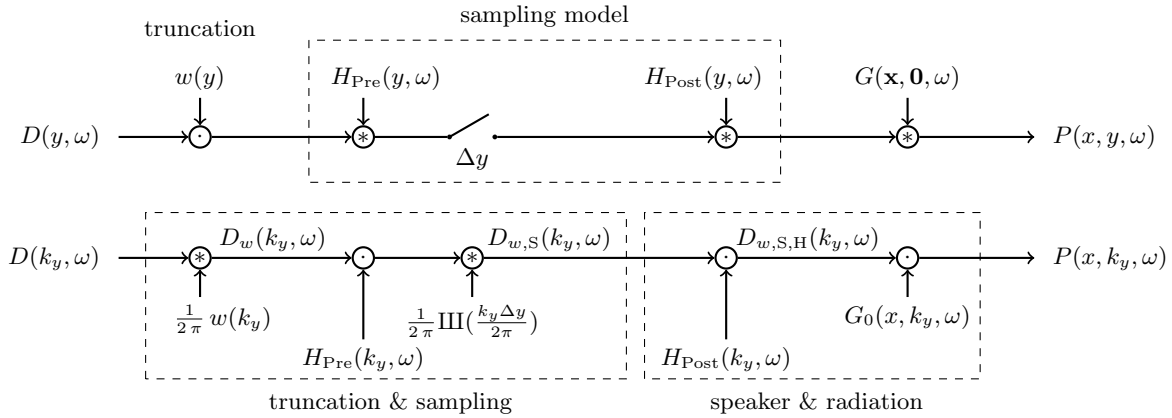

Fig. 3: The single layer potential for a linear, spatially discretized and truncated SSD. Representation in spatial (top) and angular spectrum domain (bottom), cf. [6, Fig. 5.7], [6, Fig. 5.13]. Convolution is denoted by $\circledast$, multiplication by $\odot$.

is generated. For all other μ that fulfill $|\mu\,\Delta k_y| < \frac{\omega}{c}$ propagating cylindrical waves are synthesized that manifest as spatial aliasing, cf. [1, Fig. 2(c,d)]. For $\Delta y < \lambda$ the Green's function generates a propagating wave only for $\mu = 0$ and thus no spatial aliasing occurs. By introducing the postfilter of pistons, the sound field is given as

$$P(x,y,\omega) = \frac{1}{\Delta y}\,2\,\pi\,\delta(\omega-\omega_{\mathrm{CW}})\times \sum_{\mu=-\infty}^{+\infty} H_{\mathrm{Post}}(k_y=\mu\,\frac{2\,\pi}{\Delta y},\omega)\cdot G_0(x,k_y=\mu\,\frac{2\,\pi}{\Delta y},\omega)\times \mathrm{e}^{-\mathrm{j}\,\mu\,\frac{2\,\pi}{\Delta y}\,y}. \tag{14}$$

The postfilter attenuates the spatial aliasing contributions, cf. [1, Fig. 5]. Perfect reconstruction for all temporal frequencies, i.e. a spatial-aliasing-free sound field is achieved with line pistons for $l = \Delta y$, as discussed in [1, Sec. 5.2].

4. FINITE LENGTH, CONTINUOUS LSA

To account for a finite length array, the signal processing model is extended by windowing the driving function, cf. Fig. 3. This section discusses a finite, albeit continuous SSD: the sampling stage is omitted and the driving function is truncated to

$$D_w(y,\omega) = w(y)\cdot D(y,\omega) \tag{15}$$

by employing the rectangular window (as in [2])

$$w(y) = \begin{cases} 1 \;\text{ for }\; |y| \le \frac{L}{2} \\ 0 \;\text{ else} \end{cases}, \tag{16}$$

with the angular spectrum (normalized to unity)

$$w(k_y) = \frac{\sin\left(k_y\,\frac{L}{2}\right)}{k_y\,\frac{L}{2}}. \tag{17}$$

The convolution of (17) and (5)

$$D_w(k_y,\omega) = \frac{1}{2\,\pi}\,w(k_y) *_{k_y} D(k_y,\omega) \tag{18}$$

leads to

$$D_w(k_y,\omega) = \frac{\sin\left(k_y\,\frac{L}{2}\right)}{k_y\,\frac{L}{2}}, \tag{19}$$

where we omit the dependence on $2\,\pi\,\delta(\omega-\omega_{\mathrm{CW}})$ from here on. Similar to (12) the angular spectrum of the synthesized sound field is given by

$$P(x,k_y,\omega) = D_w(k_y,\omega)\cdot G_0(x,k_y,\omega). \tag{20}$$

The Dirac function (5) is smeared by convolution (18) and the driving function's angular spectrum (19) becomes continuous regarding k_y, cf. [11, Sec. VII]. Hence, the treatment and the interpretation of the synthesized sound fields and the radiation characteristics of the LSA becomes more demanding.

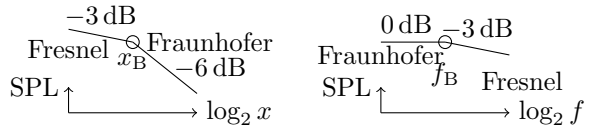

Fig. 4: Simplified radiation characteristics on x-axis for a rectangular windowed, continuous LSA under constant volume acceleration.

4.1. Farfield Directivity & Fresnel/Fraunhofer Transition

The single layer potential [1, (2)], [11, (9)]

$$P(\mathbf{x},\omega) = \int_{-\infty}^{+\infty} w(y)\, D(y,\omega)\, \frac{\mathrm{e}^{-\mathrm{j}\,\frac{\omega}{c}\,\|\mathbf{x}-\mathbf{x_0}\|}}{4\,\pi\,\|\mathbf{x}-\mathbf{x_0}\|}\,\mathrm{d}y \quad (21)$$

formulates the problem in the spatial domain. Closed form solutions for finite length arrays are only available for special cases.

Evaluating (21) for $\|\mathbf{x}\| \gg L$, $\|\mathbf{x}\| \gg \lambda$, $\frac{\|\mathbf{x}\|}{L} \gg \frac{L}{\lambda}$ using $\|\mathbf{x}\| = r = \text{const}$, the farfield polar pattern can be analytically derived [25, Ch. 3.5], and the direct link to the angular spectrum

$$P(r,\varphi,\omega) \propto D_w(k_y,\omega) = \int_{-\infty}^{+\infty} D_w(y,\omega)\,\mathrm{e}^{+\mathrm{j}\,k_y\,y}\,\mathrm{d}y \quad (22)$$

is well known. $D_w(k_y,\omega)$ is therefore interpreted as the farfield directivity of the LSA cf. [23, Ch. 7.11], [22, Ch. 26.2], [25, Ch. 3.6].

Another closed form solution of (21) can be derived for positions $\mathbf{x} = [x, 0, 0]^T$, $x \geq L/2$, i.e. along the main axis, cf. [22, Ch. 26.23], [26], [2, I.3.b]. The latter two papers deduced that a continuous, finite length array with constant volume acceleration exhibits a *Fresnel* region (3 dB amplitude loss per distance doubling with ripples, 3 dB/oct. lowpass for temporal frequencies with ripples) and a *Fraunhofer* region (6 dB amplitude loss per distance doubling, temporal frequency independent amplitude), cf. Fig. 4, [2, 26]. The transition or border distance x_B between both regions on the main axis is highly dependent on the frequency and array length. By the geometric diffraction approach the authors of [2], [3, p. 913] derived

$$x_\mathrm{B} = \frac{1}{2}\,L^2\,\frac{f}{c}\,\sqrt{1-\frac{1}{(\frac{f}{c}\,L)^2}}, \quad (23)$$

for which $x_\mathrm{B} \notin \mathbb{R}$ indicates pure Fraunhofer radiation. We therefore cannot expect cylindrical wave radiation for all frequencies, contrasting to the case for the infinite line source [26, p.12], [1].

In the following section we utilize the signal processing framework within angular spectrum domain to derive another, yet consistent viewpoint of Fresnel/Fraunhofer transition.

4.2. Angular Spectrum Synthesis

The inverse spatial Fourier transform of (20) for the propagating part of the sound field is given by

$$\begin{aligned} P(x,y,\omega) &= \mathcal{F}^{-1}_{|k_y|\leq\frac{\omega}{c}}\{D_w(k_y,\omega)\cdot G_0(x,k_y,\omega)\} \\ &= \frac{1}{2\,\pi}\int_{-\frac{\omega}{c}}^{+\frac{\omega}{c}} D_w(k_y,\omega)\cdot G_0(x,k_y,\omega)\cdot\mathrm{e}^{-\mathrm{j}\,k_y\,y}\,\mathrm{d}k_y. \end{aligned} \quad (24)$$

The analytical solution of the integral is–if feasible at all–not straightforward and we leave this for future inspection. Numerical evaluation allows for synthesizing the sound field by weighted superposition of cylindrical waves with propagating angles $-\pi/2 < \varphi < +\pi/2$, which can be interpreted as angular spectrum synthesis. Note that these waves stem from an infinite, continuous line source. The integration over k_y, i.e. the different radiation angles, yields the radiation characteristics of a line source with finite dimension by interference phenomena. This viewpoint is in contrast to the numerical evaluation of (21), which can be interpreted as source synthesis by weighted spherical monopoles.

Note that (21) inherently includes evanescent waves, which we discarded in (24) for ease of discussion. The discretization of k_y in (24) for numerical evaluation leads to spatial repetitions of the sound field along the y-axis, which must become negligible in the evaluated listener area.

Writing out (24) yields

$$P(x,y,\omega) = \frac{-\mathrm{j}}{8\,\pi}\times \int_{-\frac{\omega}{c}}^{+\frac{\omega}{c}} \frac{\sin\left(k_y\,\frac{L}{2}\right)}{k_y\,\frac{L}{2}} \cdot H_0^{(2)}\left(\sqrt{(\frac{\omega}{c})^2 - k_y^2}\cdot x\right)\cdot \mathrm{e}^{-\mathrm{j}\,k_y\,y}\,\mathrm{d}k_y. \tag{25}$$

For less computational load the large argument approximation of the Hankel function may be utilized

$$P(x,y,\omega) = \frac{-\mathrm{j}}{8\,\pi}\int_{-\frac{\omega}{c}}^{+\frac{\omega}{c}} [\frac{\sin\left(k_y\,\frac{L}{2}\right)}{k_y\,\frac{L}{2}}\times \sqrt{\frac{2}{\pi\,\sqrt{(\frac{\omega}{c})^2 - k_y^2}\cdot x}}\,\mathrm{e}^{-\mathrm{j}\left(\sqrt{(\frac{\omega}{c})^2-k_y^2}\cdot x - \frac{\pi}{4}\right)}\,\mathrm{e}^{-\mathrm{j}\,k_y\,y}\,]\,\mathrm{d}k_y \tag{26}$$

for $\sqrt{(\frac{\omega}{c})^2 - k_y^2}\cdot x \gg 1$.

The proposed framework provides an interesting opportunity, by definition of a perfect spatial lowpass filter (cf. [14, (4.55)], [12, (9)])

$$H_{\mathrm{LP}}(k_y,\omega) = \begin{cases} 1 & |k_y| < |\frac{2\pi}{L}| \\ 0 & \text{elsewhere}\,, \end{cases} \tag{27}$$

that may be included to the signal flow. This was discussed in [14, Ch. 4.6.6], [12], although with the different motivation to suppress discretization effects (spatial aliasing) instead of truncation artifacts as in the case presented here. The cutoff wave numbers $k_y = \pm 2\,\pi/L$ are the locations of the first zeros of the array's farfield directivity (19), if they exist in the *visible region* $|k_y = \pm 2\,\pi/L| < \frac{\omega}{c}$ for the chosen frequency. The spatial lowpass can be used to independently synthesize the sound field of the main lobe

$$P_{\mathrm{main}}(x,y,\omega) = \mathcal{F}^{-1}_{|k_y|\le\frac{\omega}{c}}\{H_{\mathrm{LP}}(k_y,\omega)\cdot D_w(k_y,\omega)\cdot G_0(x,k_y,\omega)\} \tag{28}$$

and that of the remaining propagating side lobes

$$P_{\mathrm{side}}(x,y,\omega) = \mathcal{F}^{-1}_{|k_y|\le\frac{\omega}{c}}\left\{\left(1-H_{\mathrm{LP}}(k_y,\omega)\right)\cdot D_w(k_y,\omega)\cdot G_0(x,k_y,\omega)\right\}. \tag{29}$$

This is equivalent to splitting the integral (25) into three integration ranges

$$P(x,y,\omega) = \underbrace{\int_{-\frac{2\,\pi}{L}}^{+\frac{2\,\pi}{L}} \ldots}_{P_{\mathrm{main}}(x,y,\omega)} + \underbrace{\int_{-\frac{\omega}{c}}^{-\frac{2\,\pi}{L}} \ldots + \int_{+\frac{2\,\pi}{L}}^{+\frac{\omega}{c}} \ldots}_{P_{\mathrm{side}}(x,y,\omega)}. \tag{30}$$

4.3. Numerical Evaluation

In Fig. 5 the introduced approach is evaluated for the case $L = 8\cdot\lambda = 5.05\,\mathrm{m}$. Fig. 5a shows the sound fields' pressure level of the uniformly driven LSA in the xy-plane according to (25), (30). The sound pressure level (SPL) is normalized to 94 dB at $x = 20$ m on the main axis. The colormap is clipped for values $> 112\,\mathrm{dB_{SPL}}$ and $< 67\,\mathrm{dB_{SPL}}$. The Fresnel/Fraunhofer transition distance (23) for this example is given to $x_{\mathrm{B}} = 20.04\,\mathrm{m}$. Fig. 5b shows the sound fields' pressure level that stems only from the main lobe (28), whereas Fig. 5c excludes it, i.e. the synthesis of all remaining side lobes (29). The superposition of $P_{\mathrm{main}}(x,y,\omega)$ Fig. 5b and $P_{\mathrm{side}}(x,y,\omega)$ Fig. 5c results in the sound field $P(x,y,\omega)$ Fig. 5a by interference. In Fig. 6 the SPL on the main axis was evaluated for all three cases. The main lobe sound field exhibits a ripple free amplitude decay with a transition at x_{B} from almost ideal cylindrical (Fresnel) to spherical (Fraunhofer) wave propagation. The sound field that excludes the main lobe exhibits lower overall SPL, notches and an amplitude loss, that is larger than 6 dB per distance doubling for $x > x_{\mathrm{B}}$. The interaction of the main and side lobes for $x < x_{\mathrm{B}}$ results in the rippled on-axis sound pressure level that is typical for the Fresnel region [2, 21, 26]. The total sound field in the xy-plane is corrupted by the side lobes as long as the level of the latter is large enough to produce perturbing interferences. The side lobe level attenuation for $x > x_{\mathrm{B}}$ is larger than 20 dB, and thus has weak impact on the total sound field, which is expected in the Fraunhofer region.

By observing the temporal frequency and LSA length dependence regarding the integration limits for the main lobe sound field

$$|k_y = \sin\varphi\,\frac{\omega}{c}| = \frac{2\,\pi}{L}, \tag{31}$$

it becomes obvious that for higher frequencies and/or larger LSAs, the side lobe field is synthe-

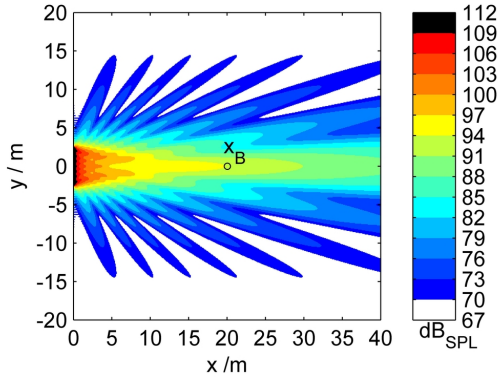

(a) Complete sound field $|P(x,y,\omega)| = |P_{\text{main}}(x,y,\omega) + P_{\text{side}}(x,y,\omega)|$ according to (25),(30)

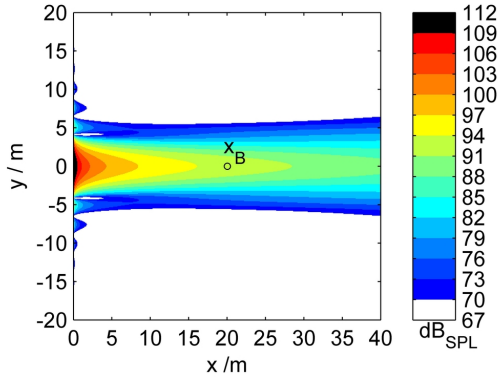

(b) $|P_{\text{main}}(x,y,\omega)|$ (28) of main lobe components.

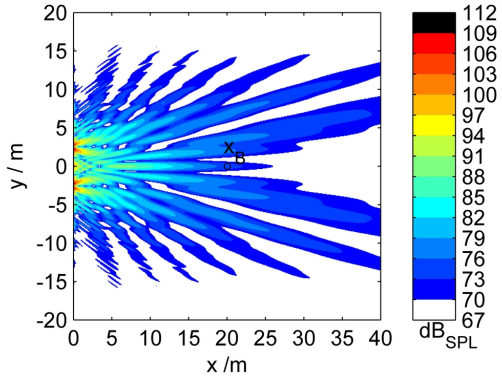

(c) $|P_{\text{side}}(x,y,\omega)|$ (29) of side lobe components.

Fig. 5: Level of sound field $|P(x,y,\omega)|$ (top) synthesized by numerical evaluation of (25) with a continuous, finite length array ($L = 5.05\,\text{m}$, $f = 8 \cdot c/L = 543.4\,\text{Hz}$).

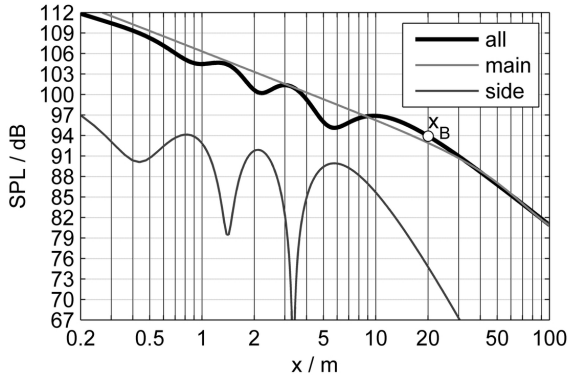

Fig. 6: On-axis sound pressure level for Fig. 5.

sized from smaller radiation angles φ. These waves closer to $\varphi = 0°$ interfere with the main lobe within a much larger spatial region, and this is indicating the large Fresnel/Fraunhofer transition borders in (23) for high frequencies and large array lengths.

5. FINITE LENGTH, DISCRETIZED LSA

We proceed with the discussion of a finite length, discrete LSA modeled with pistons. Therefore we employ the complete signal processing chain in Fig. 3 except the prefilter H_{Pre}. As depicted in Fig. 1, an axisymmetric LSA geometry with regard to $y = 0$ and an odd number N of sources is assumed.

The driving function for a finite length, uniformly driven and discretized array of spherical monopoles is modeled as

$$D_{w,\text{S}}(y,\omega) = \sum_{\mu=-\frac{N-1}{2}}^{+\frac{N-1}{2}} \delta(y - \mu\,\Delta y). \qquad (32)$$

This includes spatial truncation (15) by a rectangular window (16) and discretization with step size Δy (6). The corresponding angular spectrum is given as

$$D_{w,\text{S}}(k_y,\omega) = \sum_{\mu=-\frac{N-1}{2}}^{+\frac{N-1}{2}} \mathrm{e}^{+\mathrm{j}\,(k_y\,\Delta y)\,\mu}. \qquad (33)$$

This geometric series has the closed form solution of the Dirichlet kernel, also called aliased sinc-function [27, (3-37) ff., App. B], given by

$$D_{w,\text{S}}(k_y,\omega) = \frac{1}{N}\frac{\sin(k_y\,\Delta y\,N/2)}{\sin(k_y\,\Delta y/2)}, \qquad (34)$$

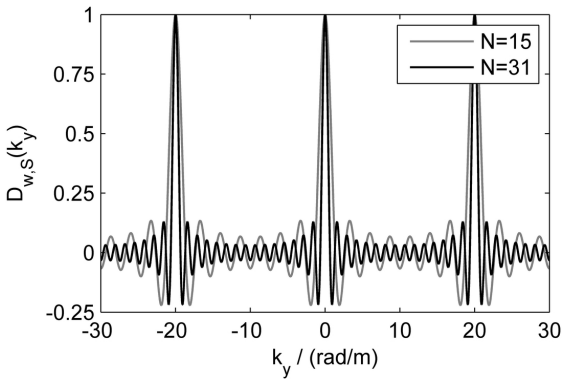

Fig. 7: $D_{w,\mathrm{S}}(k_y)$ in (34) for $\Delta y = 2\,\pi/20\,\mathrm{m}$, $\Delta k_y = 20\,\mathrm{rad/m}$, $N = 15$ (gray), $N = 31$ (black).

using unit amplitude normalization for ease of discussion, cf. [22, Ch. 26.3.2], [23, Ch. 7.8], [19, Ch. 6.3]. $D_{w,\mathrm{S}}(k_y)$ in (34) is formally defined for all $k_y \in \mathbb{R}$. We see that for

$$k_y = \mu\,\frac{2\,\pi}{\Delta y} = \mu\,\Delta k_y \tag{35}$$

unit amplitude peaks occur due to the spectral repetitions of the Dirac comb in (6). The Dirac comb is smeared to sinc-like lobes due to windowing. The main lobe is located between $k_y = \pm 2\,\pi/L$ as in Sec. 4, the lobes between $k_y = \mu\,\Delta k_y \pm 2\,\pi/L$ for $\mu \neq 0$ are termed grating lobes [19], whereas the remaining side lobes exhibit a sinc-like decay, cf. [2, p.15]. Thus, a higher number of sources N and thereby a longer LSA exhibits narrower main and grating lobes, cf. Fig. 7. A smaller discretization step Δy results in a larger distance Δk_y between the adjacent main/ grating lobes. The propagating region of the Green's function's angular spectrum is triggered by (34) with the frequency dependent visible region $-\frac{\omega}{c} < k_y < +\frac{\omega}{c}$.

In [2, II.2.a] (34) was termed *form factor* of the array, whereas in [21] the term *directivity function* was used. The angular spectrum (34) is interpreted as the farfield directivity of a finite length line array build with equidistantly spaced spherical monopoles.

According to the signal processing model, when using pistons instead of spherical monopoles, we can define the driving function's angular spectrum

$$D_{w,\mathrm{S,H}}(k_y,\omega) = D_{w,\mathrm{S}}(k_y,\omega)\cdot H_{\mathrm{post}}(k_y,\omega) \tag{36}$$

as the farfield directivity of the LSA, which is consistent with the product theorem [15, Ch. 7], [23, Ch. 7.9]. In [2, p.13], [2, Fig. 16] the farfield of a discrete, finite length array was termed *collective Fraunhofer region*. In antenna design the product (36) was termed *final array factor* for a closely related problem treatment [28].

For a line piston LSA with $\Delta y = l$ and $L = N \cdot l$, we arrive at

$$D_w(k_y,\omega) = D_{w,\mathrm{S}}(k_y,\omega)\cdot H_{\mathrm{Rect}}(k_y,\omega) \tag{37}$$

using (34) and (8). This yields the farfield directivity (19) of a continuous, finite length array. Note that (37) is only valid for an uniformly driven array.

At this stage of discussion it is worth to stress that manipulation of $D_{w,\mathrm{S}}(k_y,\omega)$ (34) and $D_{w,\mathrm{S,H}}(k_y,\omega)$ (36) in the electronic signal domain is not possible. The postfilter acts in the acoustic domain and once the driving function is physically sampled by using discrete loudspeakers there is no further control over $D_{w,\mathrm{S}}(k_y,\omega)$ and $D_{w,\mathrm{S,H}}(k_y,\omega)$ in the electronic domain.

5.1. First and Second WST Criterion

The previous introduction of the driving function for a finite length, discretized array and the product theorem allows for revision of the 1st and 2nd WST criteria. The revision of the other three WST criteria [3, p.929] is beyond the scope of this paper.

According to the sampling theorem for basisband signals, perfect reconstruction of (34) requires an ideal spatial lowpass with Nyquist band width

$$H_{\mathrm{LP}}(k_y,\omega) = \begin{cases} 1 & |k_y| < \frac{\Delta k_y}{2} \\ 0 & \text{elsewhere} \end{cases} \tag{38}$$

as the postfilter. The finite length line array build with equidistantly spaced spherical monopoles does not involve this filter physically. This models practical LSA designs using approximately omnidirectional radiating loudspeakers at low frequencies. Perfect reconstruction is thus only possible for frequencies that fulfill

$$|k_y| = \frac{\omega}{c} < \frac{\Delta k_y}{2}. \tag{39}$$

Rearranging (39) reveals the 2nd WST criterion [2], [3, p.918], [22, Ch. 26.4]

$$\text{WST \#2:} \qquad f < \frac{c}{2\,\Delta y} \quad \leftrightarrow \quad \Delta y < \frac{\lambda}{2}, \tag{40}$$

that defines a spherical monopole spacing not larger than half of the radiated wave length in order to synthesize a spatial-aliasing-free sound field. Eq. (40) requires very small distances Δy and thus small individual drivers for high frequencies, which is a technically demanding approach.

Therefore the 1st WST criterion was defined for the case that (34) exceeds the Nyquist band width for high frequencies. With regard to the signal processing model in Fig. 3, a postfilter H_{Rect} was introduced by the authors of [2], cf. [3, Fig. 6]. By allowing grating lobes in the region of $|k_y| < \frac{\omega}{c}$ in (34), spatial aliasing is tolerated. This is in contrast to complete avoidance by fulfillment of the 2nd WST criterion. For large N the Active Radiation Factor (ARF) [3, Ch. 3.2]

$$\text{WST \#1:} \qquad \mathrm{ARF} = \frac{l}{\Delta y} \geq 0.82 \tag{41}$$

was defined, such that the farfield level of all side lobes (i.e. from windowing) and grating lobes (from sampling) in (36) is at least 13.5 dB below the main lobe level. This was motivated with amplitude matching of the highest side lobe of a continuous, rectangular windowed array. We define the ARF for the practical setup of a finite length LSA with line pistons to

$$\mathrm{ARF} = \frac{N \cdot l}{L} \geq 0.82 \tag{42}$$

according to the sketched geometry in Fig. 1 and recall that (37) corresponds to an ARF = 1 design.

For the two-dimensional case of adjacent circular pistons with radius r_0 the ARF was derived to [3]

$$\mathrm{ARF} = \frac{\pi\, r_0^2}{4\, r_0^2} \approx 0.7854, \tag{43}$$

using a quadratic enclosure with length $2\, r_0$. It was concluded that the 1st WST criterion never can be fulfilled by usage of circular pistons, which inherently suggests that only the 2nd one can be used for circular pistons. The interpretation is misleading, since the criterion was derived for utilizing a line piston postfilter.

Although – for an infinite array – it was shown that H_{Circ} cannot perfectly suppress the undesired spectral repetitions for $\Delta y = 2\, r_0$ [1, Fig. 5] as H_{Rect} does for $l = \Delta y$ [1, Fig. 7], H_{Circ} has better spatial lowpass characteristics than H_{Rect} with the same dimension ($l = 2\, r_0$), for the case that spatial aliasing is disregarded, cf. Fig. 2. A comparison of two LSAs with

- 3" circular pistons, ARF $= \pi/4$
- line pistons of length $l = 0.0635\,\mathrm{m}$, ARF $= 0.82$

of same LSA length $L \approx 5\,\mathrm{m}$ is conducted. The line piston LSA fulfills the 1st WST criterion, whereas the circular piston LSA violates both the 1st WST criterion (due to insufficient ARF) and the 2nd WST criterion (due to high frequency). In Fig. 8 the farfield directivities $|D_{w,\mathrm{S}}(k_y,\omega) \cdot H_{\mathrm{post}}(k_y,\omega)|$ for 5 kHz are depicted. The discretization step size Δy is almost equal for both cases and the same number of pistons $N = 65$ is used. Due to equal LSA length the main lobes exhibits the same sinc-patterns. Two grating lobes of (34) exist in the visible region $-\frac{\omega}{c} < k_y < +\frac{\omega}{c}$ and are attenuated by the postfilters. Fig. 8 indicates the larger grating lobe suppression at $|k_y = 2\,\pi/\Delta y| \approx 80\,\mathrm{rad/m}$ for the circular piston LSA of about 15 dB, compared to the expected 13.5 dB for the line piston LSA.

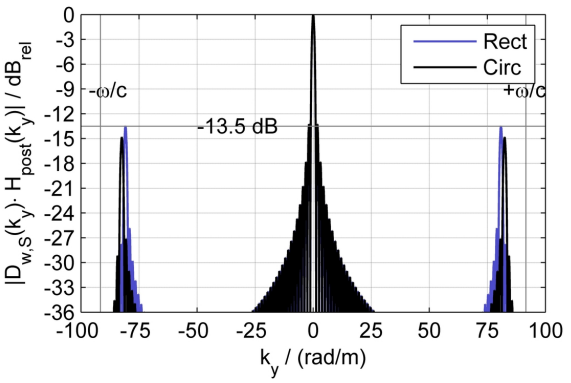

Fig. 8: $|D_{w,\mathrm{S,H}}(k_y,\omega)|$ for $f = 5\,\mathrm{kHz}$, $L \approx 5\,\mathrm{m}$. LSA with $\mathrm{ARF}_{\mathrm{Circ}} = \pi/4$: $r_0 = 3"/2$, $\Delta y = 3"$, $N = 65$. LSA with $\mathrm{ARF}_{\mathrm{Rect}} = 0.82$: $l = 0.0635\,\mathrm{m}$, $\Delta y = 0.0777\,\mathrm{m}$, $N = 65$.

5.2. Numerical Evaluation

The angular spectrum of the synthesized sound field is with (36) given as, cf. (12)

$$P(x,k_y,\omega) = D_{w,\mathrm{S,H}}(k_y,\omega) \cdot G_0(x,k_y,\omega). \tag{44}$$

The inverse spatial Fourier transform for the range $|k_y| < \frac{\omega}{c}$ yields the sound field for propagating waves

similar to (24)

$$P(x,y,\omega) = \mathcal{F}^{-1}_{|k_y|\leq\frac{\omega}{c}}\{P(x,k_y,\omega)\} = \frac{1}{2\,\pi}\cdot\int_{-\frac{\omega}{c}}^{+\frac{\omega}{c}}[D_{w,\mathrm{S}}(k_y,\omega)\cdot H_{\mathrm{post}}(k_y,\omega) \times G_0(x,k_y,\omega)\cdot \mathrm{e}^{-\mathrm{j}\,k_y\,y}]\,\mathrm{d}k_y. \quad (45)$$

By using (45), a 5 m-LSA modeled with line pistons is numerically evaluated according to the strategy in (30). The LSA parameters in Fig. 14a are used for $f = 1.2\,\mathrm{kHz}$. Note that the evaluation is only valid in the farfield of the line pistons. The sound fields' pressure levels are visualized in Fig. 9. The farfield directivity exhibits two grating lobes around $\pm k_y = 13.6861\,\mathrm{rad/m}$, $\varphi = \pm 38.5°$, that have been attenuated by the line piston's postfilter, cf. Fig. 14a. The resulting spatial aliasing is observed in Fig. 9a. In the plotted region of Fig. 9b $P_{\mathrm{main}}(x,y,\omega)$ exhibits pure Fresnel characteristics on main axis. This sound field is corrupted by interference with $P_{\mathrm{side}}(x,y,\omega)$ that is shown in Fig. 9c. This results in the so-called *chaotic region* [2, II.1. & fig. 16] close to the array. Note that this is a deterministic phenomenon due to (45). In [2, p. 14, r^2_{Border}] the transition distance on main axis between the chaotic region and the collective Fraunhofer region was derived from the geometric diffraction approach to

$$x_{\mathrm{B}} = \frac{1}{2}\,N^2\,\Delta y^2\,\frac{f}{c} - \frac{1}{4\,\frac{f}{c}}. \quad (46)$$

For $x > x_{\mathrm{B}}$ the side lobe level becomes negligible, which is confirmed by the on-axis sound pressure level depicted in Fig. 10. For the chosen example $x_{\mathrm{B}} = 44.5\,\mathrm{m}$ holds.

It is worth realizing the fundamental difference regarding the synthesized sound fields of infinite and finite length LSAs. While for infinite arrays the sound field remains corrupted over the whole space, the finite length LSA exhibits an almost spatial-aliasing-free sound field beyond the discussed distance x_{B}.

5.2.1. Circular vs. Line Piston LSA

In the remainder of Sec. 5 we discuss further properties and special cases for uniformly driven, discrete, finite LSAs. The simulation results are depicted in Fig. 13 to Fig. 15 at the end of this paper. In those figures one column represents a specific

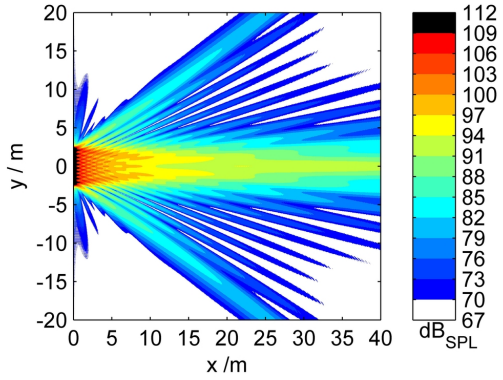

(a) Complete sound field $|P(x,y,\omega)| = |P_{\mathrm{main}}(x,y,\omega) + P_{\mathrm{side}}(x,y,\omega)|$.

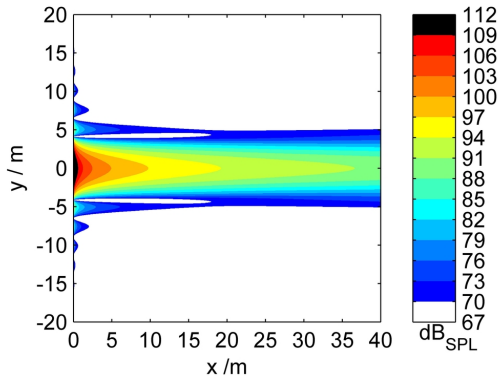

(b) $|P_{\mathrm{main}}(x,y,\omega)|$ of main lobe components.

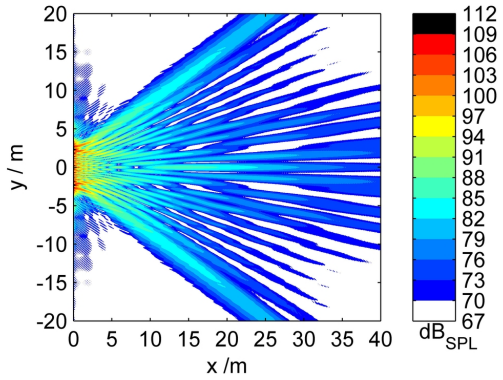

(c) $|P_{\mathrm{side}}(x,y,\omega)|$ of side lobe components.

Fig. 9: Sound field synthesized by numerical evaluation of (45) with an LSA build by line pistons ($L = 4.9684\,\mathrm{m}$, $f = 1.2\,\mathrm{kHz}$, $\Delta y = 0.4591\,\mathrm{m}$, $l = 0.381\,\mathrm{m}$, ARF=0.8436, $N = 11$).

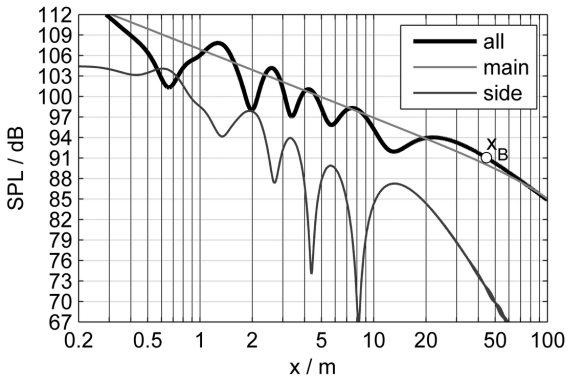

Fig. 10: On-axis sound pressure level for Fig. 9.

scenario. Subplot a) depicts the farfield directivity $|D_{w,\mathrm{S,H}}(k_y,\omega)|$ over temporal frequency f and wave number k_y. Levels < -36 dB are clipped to white color. Subplot b) shows the specific farfield directivity for a chosen frequency, for which in subplot c) the resulting sound field is numerically evaluated by (21). All sound fields' levels are normalized to $94\,\mathrm{dB_{SPL}}$ at $x = 10\,\mathrm{m}$ on main-axis. Sound pressure levels > 112 dB are clipped to black color, those $< 76\,\mathrm{dB_{SPL}}$ to white color. The frequencies for the synthesized sound fields were chosen to highlight the particular phenomenon under discussion.

In Fig. 13 LSAs with ARF $= \pi/4$, $L \approx 5\,\mathrm{m}$ modeled with circular (left) and line (right) pistons of about the same dimensions can be compared. The circular piston LSA – although violating the 1st and 2nd WST criterion – has better spatial lowpass characteristics, the two observable grating lobes in Fig. 13c for 1.6 kHz are attenuated ≈ 15 dB in the far field. For $20 < |k_y| < 30\,\mathrm{rad/m}$ side lobe suppression of more than 36 dB is observed. This results in only small sound pressure levels in the proximity above and below the LSA. Using line pistons for this LSA on the other hand violates the ARF criterion (41): we observe four prominent grating lobes in Fig. 13d, postfilter attenuation of minimum 13.5 dB is not achieved for the first pair. The outermost grating lobes produce high sound pressure level in the depicted sound field near above and below the LSA.

For the discussed case the circular piston LSA exhibits less spatial aliasing, as was already discussed in Sec. 5.1. The result here is however only of theoretical interest, since a 15" circular piston is not able to radiate uniformly at this frequency in practice and the farfield piston model is not valid. However, choosing very small drivers and a source spacing in the range of few cm for the high frequency LSA section–and thereby fulfilling the sampling theorem (39)–is a recently realized approach in commercial LSA designs.

5.2.2. LSAs with Different Line Piston Length

The ARF criterion (41) alone states only a minimum ratio for piston size and source spacing, which obviously can be met by different setups. In Fig. 14 two LSAs with ARF ≈ 0.84 and $L \approx 5\,\mathrm{m}$ modeled with line pistons, using $N = 11$ pistons of length $l = 0.381\mathrm{m}$ (left) and $N = 21$ with $l = 0.2012\mathrm{m}$ (right) are visualized. The $\mathrm{LSA}_{N=11}$ exhibits four grating lobes for $f = 1.6\,\mathrm{kHz}$ due to the larger discretization step Δy, concurrently with high suppression in the range of $k_y \approx 20\,\mathrm{rad/m}$. The $\mathrm{LSA}_{N=21}$ features only two grating lobes that have about the same farfield radiation angles as the two outermost grating lobes of $\mathrm{LSA}_{N=11}$. This is due to $\Delta y_{N=11} \approx 2\,\Delta y_{N=21}$. In both cases all side and grating lobes are attenuated at least 13.5 dB in the farfield, since the ARF criterion is fulfilled.

Note that the maximum line piston size was defined only in [3, Sec. 6.2] by linking it with a maximum allowed splaying angle of adjacent pistons for curved arrays.

5.2.3. LSA with Spatial Aliasing at $\varphi = \pm 90°$

We use the same LSA setup with $N = 11$ line pistons as in the previous subsection, although at a different frequency. Evaluating at $f = 1.495\,\mathrm{kHz}$ illustrates the phenomenon of propagating waves along the array axis, depicted in the left column of Fig. 15. Here, the second spectral repetitions with $\mu = \pm 2$ occur at wave numbers $|k_y| = 27.37\,\mathrm{rad/m}$, close to the pole of $G_0(x, k_y, \omega)$ at $\frac{\omega}{c} = 27.386\,\mathrm{rad/m}$. This results in wave propagation along the array ($|\varphi| \approx 90°$). The level of the produced sound field close to the array is not predicted by the LSA farfield directivity $D_{w,\mathrm{S,H}}(k_y,\omega)$. In Fig. 11 the sound pressure level along the x- and the y-axis is evaluated. It indicates that the wave propagation along the array (grating lobe on y-axis) decays with 6 dB per distance doubling and therefore faster than the main lobe (on x-axis) that exhibits a typical Fresnel/Fraunhofer level

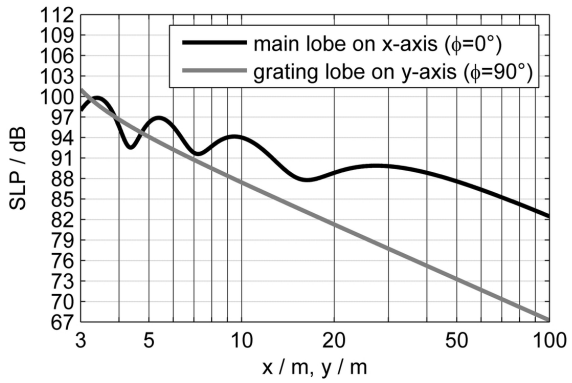

Fig. 11: On-axis and off-axis sound pressure level versus distance for Fig. 15e.

decay. However, very close to the array ($x, y < 7\,\mathrm{m}$) both sound pressure levels exhibit the same order of magnitude. In the collective Fraunhofer region ($x/y = 100\,\mathrm{rad/m}$, Fig. 11) $|D_{w,\mathrm{S,H}}(k_y, \omega)|$ predicts the grating lobe suppression of 15 dB, that is observed in Fig. 15c. Wave propagation along the array with high SPL, that results from spatial aliasing, occurs for all LSA designs that violate the 2nd WST criterion and ARF < 1. This is observable at particular frequencies, where the grating lobes trigger the Green's function's angular spectrum very close to its pole. This behavior cannot be avoided and is observable in commercial prediction software as well.

5.2.4. Spatial-Aliasing-Free LSA with ARF=1

In Fig. 15, right column for completeness a continuous LSA is simulated corresponding to Sec. 4. Due to (37) this models also a discrete LSA with ARF $= 1$ using the chosen parameters. No grating lobes occur and only the sinc-function of the truncation window (17) is observable, producing the well known sound field of a continuous, uniformly driven line source, cf. [21, Fig. 13].

6. ELECTRONICALLY STEERED, FINITE LENGTH AND DISCRETIZED LSA

Finally we briefly discuss radiation synthesis into direction $\varphi \neq 0°$. By applying a delay time τ cumulatively to the individual sources, the main lobe of an LSA can be steered into direction of φ_{Steer}. With the wave velocity along the array, cf. [25, Ch. 3.5.3]

$$c_s = \frac{\Delta y}{\tau} = \frac{c}{\sin \varphi_{\mathrm{Steer}}} > c \tag{47}$$

and the corresponding wave number $k_{y,\mathrm{Steer}} = \frac{\omega}{c_s}$, the driving function's angular spectrum for a straight, discretized, rectangular windowed and finite length array is given as [23, (7.8.16)]

$$D_{w,\mathrm{S}}(k_y, \omega) = \frac{1}{N} \frac{\sin([k_y - k_{y,\mathrm{Steer}}]\,\Delta y\, N/2)}{\sin([k_y - k_{y,\mathrm{Steer}}]\,\Delta y/2)}. \tag{48}$$

The farfield directivities $|D_{w,\mathrm{S,H}}(k_y, \omega)|$ for two electronically steered ($\varphi_{\mathrm{Steer}} = -5°$) LSAs of length

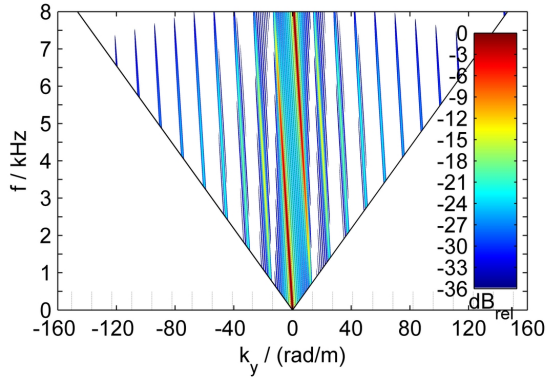

(a) Line pistons $H_{\mathrm{Rect}}(k_y, \omega)$, $l = 0.4591\,\mathrm{m}$, $L = 5.05\,\mathrm{m}$, $N = 11$, ARF=1, $\Delta y = 0.4591\,\mathrm{m}$, $\Delta k_y = 13.6859\,\mathrm{rad/m}$.

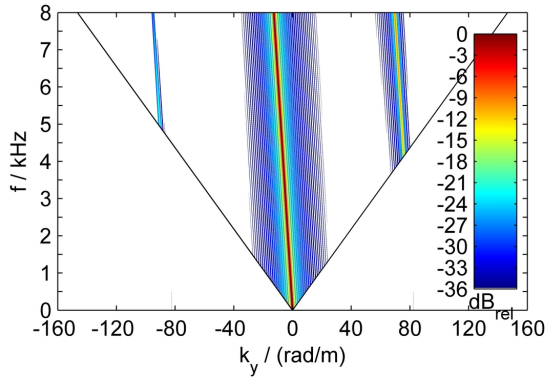

(b) 3" circular pistons $H_{\mathrm{Circ}}(k_y, \omega)$, $L = 4.9530\,\mathrm{m}$, $N = 65$, ARF=$\pi/4$, $\Delta y = 0.0762\,\mathrm{m}$, $\Delta k_y = 82.4565\,\mathrm{rad/m}$.

Fig. 12: Farfield directivities $|D_{w,\mathrm{S,H}}(k_y, \omega)|$ for off-axis beamsteering to $\varphi_{\mathrm{Steer}} = -5°$ for two LSA setups.

$L \approx 5\,\mathrm{m}$ modeled with line and circular pistons respectively are visualized in Fig. 12. The line piston LSA in Fig. 12a features an ARF=1. The circular piston LSA exhibits an ARF $= \pi/4$, with much smaller pistons than the line pistons. The line piston postfilter H_{Rect} attenuates the intended main lobe in Fig. 12a for $f > 6\,\mathrm{kHz}$ due to its first notch of the sinc function. A prominent grating lobe enters the propagating part of the Green's function's angular spectrum at about 800 Hz and can be traced towards $k_y \approx 0\,\mathrm{rad/m}$ at 8 kHz. It exhibits about the same level as the intended main lobe and will severely corrupt the desired wave propagation. Electronic beamsteering with large line pistons (large l, small Δk_y, narrow main lobes in farfield directivity) is therefore not advisable.

The electronically steered LSA in Fig. 12b is modeled with adjacent 3" circular pistons. Since the sampling step size is much smaller, only two grating lobes are observed. The intended main lobe is maintained within the plotted frequency range, due to the less directed farfield pattern of the postfilter. For an LSA modeled with pistons, it is obviously advantageous to use a larger number N of smaller sources, which exhibit a less directed piston farfield pattern and thus offer a higher degree of freedom. In essence this was confirmed in the simulations performed in [29].

7. CONCLUSION

We revised and provided new insights to the 1st and 2nd Wave Sculpture Technology criteria with a signal processing framework that was developed in sound field synthesis research. Although analytical treatment is sophisticated and presumably not possible, the numerical evaluation of–what we termed–angular spectrum synthesis allows for a more intuitive interpretation on how sound fields are synthesized from linear, discrete and finite length arrays that are modeled with farfield directivities of baffled pistons.

We conclude that spatial-aliasing-free sound fields for high frequencies should be synthesized with line source arrays that employ waveguides with an ideal active radiation factor of one. Based on the discussions it is furthermore suggested to choose a rather fine driving granularity, i.e. small, individually driven pistons. This approach would displace the spatial aliasing problem to higher temporal frequencies and therefore a higher degree of freedom with regard to electronic beamforming is achieved. This would allow improved performance of finding driving functions in recently developed numerical optimization schemes [30–32].

8. REFERENCES

[1] Schultz, F.; Rettberg, T.; Spors, S. (2014): "On spatial-aliasing-free sound field reproduction using infinite line source arrays." In: *Proc. of the 136th Audio Eng. Soc. Conv., Berlin*, #9078.

[2] Heil, C.; Urban, M. (1992): "Sound fields radiated by multiple sound sources arrays." In: *Proc. of 92nd Audio Eng. Soc. Conv., Vienna*, #3269.

[3] Urban, M.; Heil, C.; Baumann, P. (2003): "Wavefront Sculpture Technology." In: *J. Audio Eng. Soc.*, **51**(10):912–932.

[4] Berkhout, A.J.; de Vries, D.; Vogel, P. (1992): "Wave Front Synthesis: A new direction in electroacoustics." In: *Proc. of 93rd Audio Eng. Soc. Conv., San Francisco*, #3379.

[5] de Vries, D. (1996): "Sound reinforcement by wavefield synthesis: Adaptation of the synthesis operator to the loudspeaker directivity characteristics." In: *J. Audio Eng. Soc.*, **44**(12):1120–1131.

[6] Start, E.W. (1997): *Direct Sound Enhancement by Wave Field Synthesis*. Ph.D. thesis, Delft University of Technology.

[7] Spors, S. (2006): "Spatial aliasing artifacts produced by linear loudspeaker arrays used for Wave Field Synthesis." In: *Proc. of the 2nd ISCCSP, Marrakech.*

[8] Spors, S.; Rabenstein, R.; Ahrens, J. (2008): "The theory of Wave Field Synthesis revisited." In: *Proc. of the 124th Audio Eng. Soc. Conv., Amsterdam*, #7358.

[9] Verheijen, E. (2010): *Sound Reproduction by Wave Field Synthesis*. Ph.D. thesis, Delft University of Technology.

[10] Spors, S.; Ahrens, J. (2010): "Analysis and improvement of pre-equalization in 2.5-dimensional Wave Field Synthesis." In: *Proc. of the 128th Audio Eng. Soc. Conv., London*, #8121.

[11] Ahrens, J.; Spors, S. (2010): "Sound field reproduction using planar and linear arrays of loudspeakers." In: *IEEE Trans. Audio Speech Language Process.*, **18**(8):2038–2050.

[12] Ahrens, J.; Spors, S. (2010): "On the anti-aliasing loudspeaker for sound field synthesis employing linear and circular distributions of secondary sources." In: *Proc. of the 129th Audio Eng. Soc. Conv., San Francisco*, #8246.

[13] Firtha, G.; Fiala, P. (2012): "Prefiltering the wave field synthesis operators - anti-aliasing and source directivity." In: *Intl. Conference on Noise and Vibration Engineering (ISMA 2012), Leuven, Belgium*, 3121 – 3136.

[14] Ahrens, J. (2012): *Analytic Methods of Sound Field Synthesis*. Heidelberg: Springer.

[15] Ziomek, L.J. (1995): *Fundamentals of Acoustic Field Theory and Space-Time Signal Processing*. Boca Raton: CRC Press.

[16] Williams, E.G. (1999): *Fourier Acoustics, Sound Radiation and Nearfield Acoustic Holography*. London: Academic Press.

[17] Goodman, J.W. (2005): *Introduction to Fourier Optics*. Greenwood Village: Roberts & Co Publ, 3. ed.

[18] Elliot, R.S. (2003): *Antenna Theory and Design*. Hoboken: Wiley.

[19] Balanis, C.A. (2005): *Antenna Theory - Analysis and Design*. Hoboken: Wiley, 3. ed.

[20] Schultz, F.; Spors, S. (2014): "On the frequency response variation of sound field synthesis using linear arrays." In: *Proc. of 40th DAGA, Oldenburg*, 592–593.

[21] Ureda, M.S. (2004): "Analysis of loudspeaker line arrays." In: *J. Audio Eng. Soc.*, **52**(5):467–495.

[22] Skudrzyk, E. (1971): *The Foundations of Acoustics*. New York: Springer.

[23] Kinsler, L.E.; Frey, A.R.; Coppens, A.B.; Sanders, J.V. (2000): *Fundamentals of Acoustics*. Hoboken: Wiley, 4. ed.

[24] Olver, F.W.J.; Lozier, D.W.; Boisvert, R.F.; Clark, C.W. (2010): *NIST Handbook of Mathematical Functions*. Cambridge: Cambridge University Press.

[25] Möser, M. (2009): *Engineering Acoustics, An Introduction to Noise Control*. Dordrecht: Springer, 2. ed.

[26] Lipshitz, S.P.; Vanderkooy, J. (1986): "The acoustic radiation of line sources of finite length." In: *Proc. of 81st Audio Eng. Soc. Conv., Los Angeles*, #2417.

[27] Lyons, R.G. (2011): *Understanding Digital Signal Processing*. Upper Saddle River: Prentice Hall, 3. ed.

[28] Brockett, T.J.; Rahmat-Samii, Y. (2012): "Subarray design diagnostics for the suppression of undesirable grating lobes." In: *IEEE Trans. Antennas and Propagation*, **60**(3):1373–1380.

[29] Thompson, A.; Luzarraga, J. (2013): "Drive granularity for straight and curved loudspeaker arrays." In: *Proc. of the Institute of Acoustics*, 35(2).

[30] van Beuningen, G.W.J.; Start, E.W. (2000): "Optimizing directivity properties of DSP controlled loudspeaker arrays." In: *Proc. of the Institute of Acoustics*, 22(6).

[31] Thompson, A.; Baird, J.; Webb, B. (2011): "Numerically optimised touring loudspeaker arrays - Practical applications." In: *Proc. of 131st Audio Eng. Soc. Conv., New York*, #8511.

[32] Feistel, S.; Sempf, M.; Köhler, K.; Schmalle, H. (2013): "Adapting loudspeaker array radiation to the venue using numerical optimization of FIR filters." In: *Proc. of 135th Audio Eng. Soc. Conv., New York*, #8937.

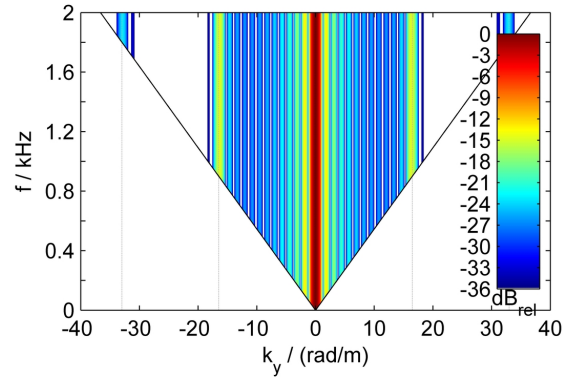

(a) $|D_{w,\mathrm{S}}(k_y,\omega)\cdot H_{\mathrm{Circ}}(k_y,\omega)|$
$r_0 = 15"/2 = 0.1905\,\mathrm{m},\ \Delta k_y = 2\,\pi/(2\,r_0) = 2\,\pi/0.381\,\mathrm{m}$

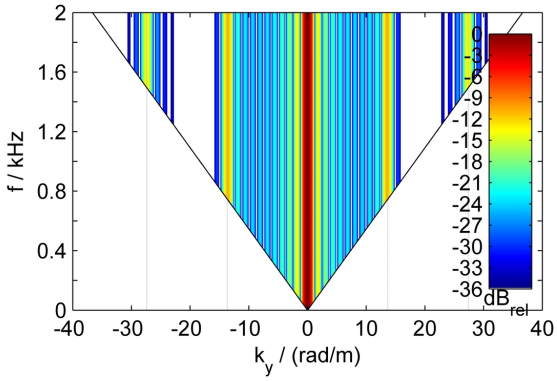

(b) $|D_{w,\mathrm{S}}(k_y,\omega)\cdot H_{\mathrm{Rect}}(k_y,\omega)|$
$l = 0.3526\,\mathrm{m},\ \Delta k_y = 2\,\pi/0.4591\,\mathrm{m}$

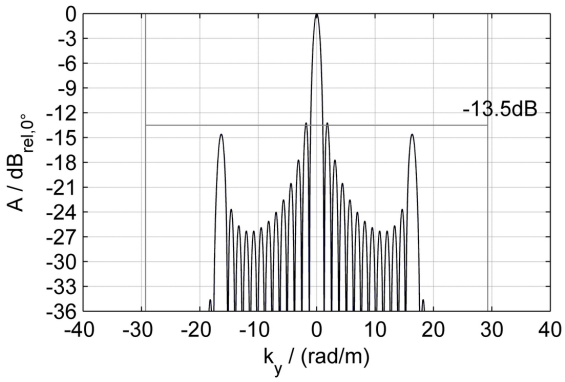

(c) $|D_{w,\mathrm{S}}(k_y,\omega)\cdot H_{\mathrm{Circ}}(k_y,\omega)|$ for $f = 1.6\,\mathrm{kHz}$

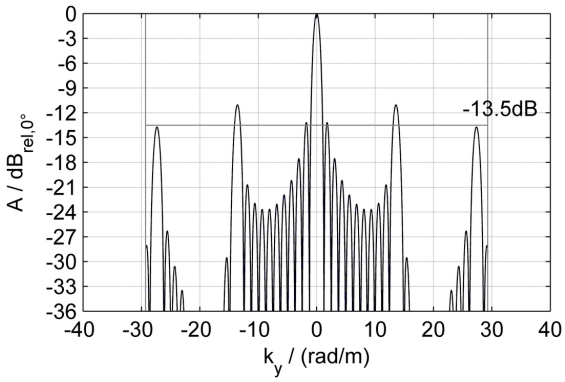

(d) $|D_{w,\mathrm{S}}(k_y,\omega)\cdot H_{\mathrm{Rect}}(k_y,\omega)|$ for $f = 1.6\,\mathrm{kHz}$

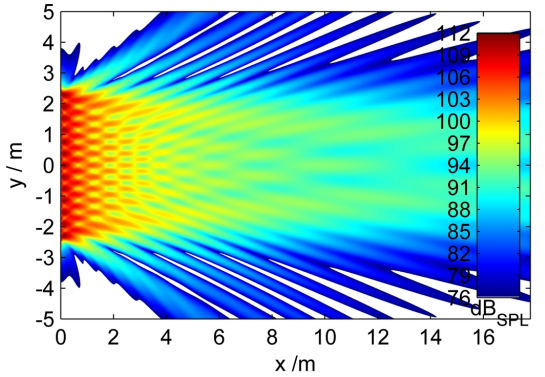

(e) sound field for $f = 1.6\,\mathrm{kHz}$ normalized to
$94\,\mathrm{dB_{SPL}}$ @ $x = 10\,\mathrm{m}, y = 0\,\mathrm{m}$

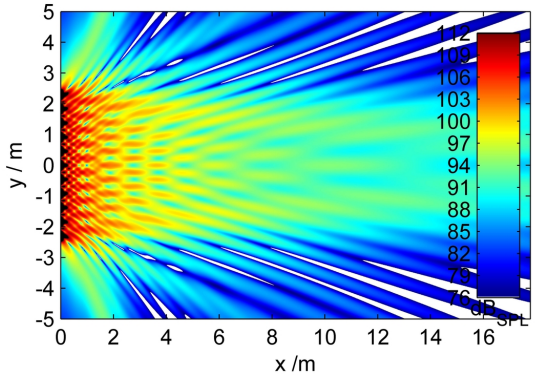

(f) sound field for $f = 1.6\,\mathrm{kHz}$ normalized to
$94\,\mathrm{dB_{SPL}}$ @ $x = 10\,\mathrm{m}, y = 0\,\mathrm{m}$

Fig. 13: Angular spectra and sound fields of a rect windowed line source array, left: with circular pistons ($L = 4.953\,\mathrm{m}$, ARF=$\pi/4$, $N = 13$), right: with line pistons ($L = 4.9401\,\mathrm{m}$, ARF=0.7851, $N = 11$)

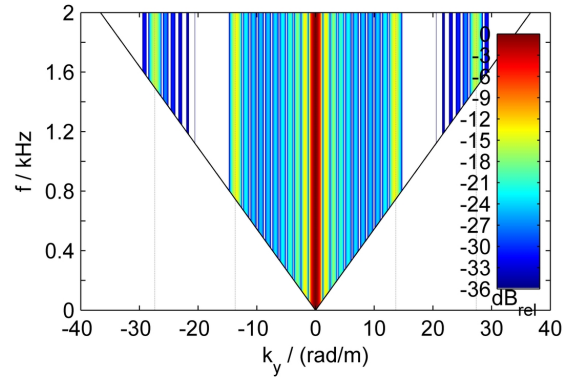

(a) $|D_{w,\mathrm{S}}(k_y,\omega)\cdot H_{\mathrm{Rect}}(k_y,\omega)|$
$l = 0.381\,\mathrm{m},\ \Delta k_y = 2\,\pi/0.4591\,\mathrm{m}$

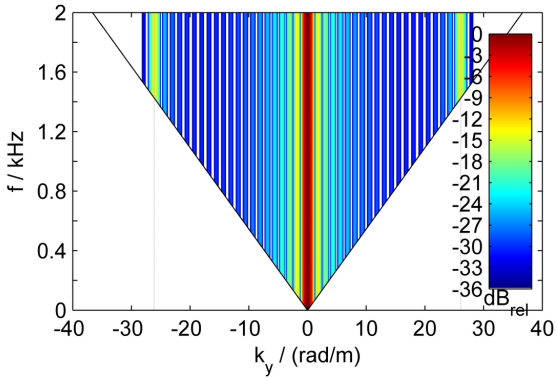

(b) $|D_{w,\mathrm{S}}(k_y,\omega)\cdot H_{\mathrm{Rect}}(k_y,\omega)|$
$l = 0.2012\,\mathrm{m},\ \Delta k_y = 2\,\pi/0.2405\,\mathrm{m}$

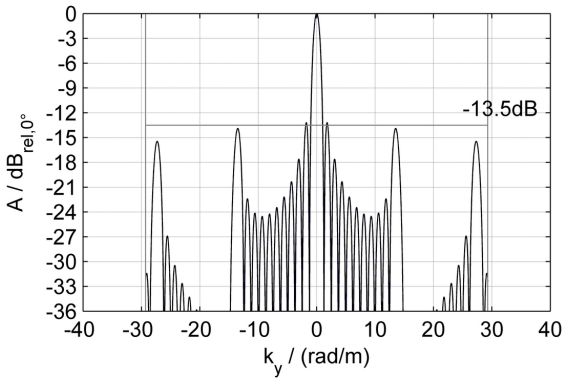

(c) $|D_{w,\mathrm{S}}(k_y,\omega)\cdot H_{\mathrm{Rect}}(k_y,\omega)|$ for $f = 1.6\,\mathrm{kHz}$

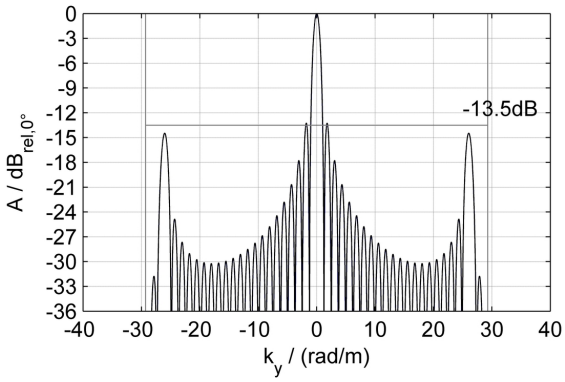

(d) $|D_{w,\mathrm{S}}(k_y,\omega)\cdot H_{\mathrm{Rect}}(k_y,\omega)|$ for $f = 1.6\,\mathrm{kHz}$

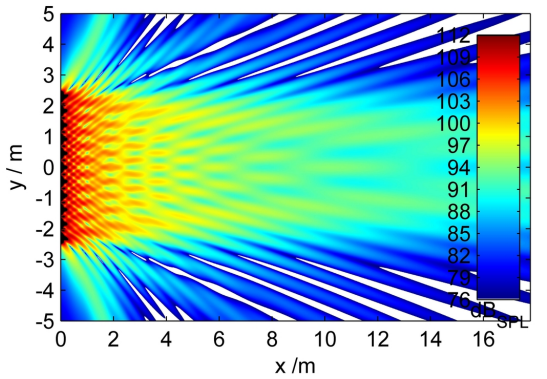

(e) sound field for $f = 1.6\,\mathrm{kHz}$ normalized to
$94\,\mathrm{dB_{SPL}}$ @ $x = 10\,\mathrm{m}, y = 0\,\mathrm{m}$

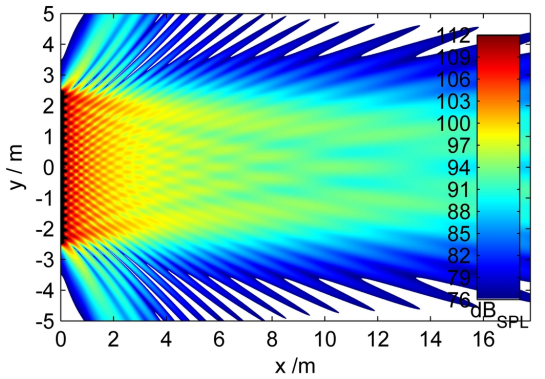

(f) sound field for $f = 1.6\,\mathrm{kHz}$ normalized to
$94\,\mathrm{dB_{SPL}}$ @ $x = 10\,\mathrm{m}, y = 0\,\mathrm{m}$

Fig. 14: Angular spectra and sound fields of a rect windowed line source array, left: with line pistons ($L = 4.9684\,\mathrm{m}$, ARF=0.8436, $N = 11$), right: with line pistons ($L = 5.0073\,\mathrm{m}$, ARF=0.8436, $N = 21$)

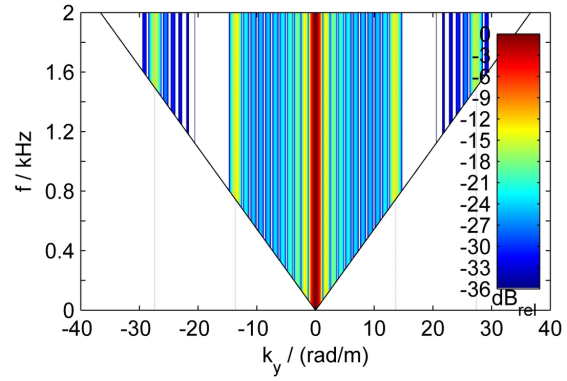

(a) $|D_{w,\mathrm{S}}(k_y,\omega)\cdot H_{\mathrm{Rect}}(k_y,\omega)|$
$l = 0.381\,\mathrm{m},\ \Delta k_y = 2\,\pi/0.4591\,\mathrm{m}$

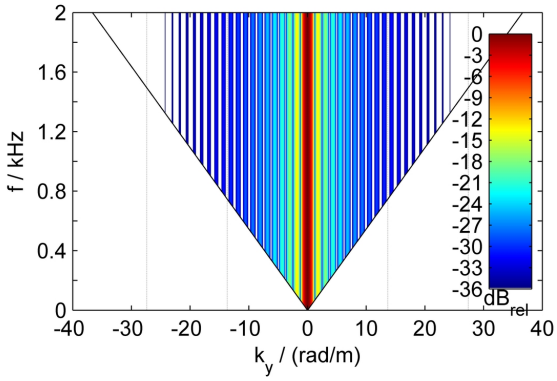

(b) $|D_{w,\mathrm{S}}(k_y,\omega)\cdot H_{\mathrm{Rect}}(k_y,\omega)|$
$l = 0.4591\,\mathrm{m},\ \Delta k_y = 2\,\pi/0.4591\,\mathrm{m}$

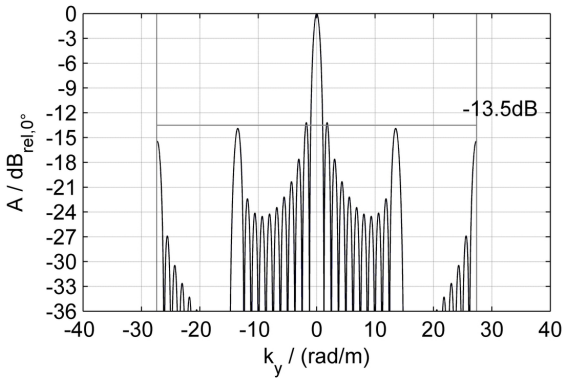

(c) $|D_{w,\mathrm{S}}(k_y,\omega)\cdot H_{\mathrm{Rect}}(k_y,\omega)|$ for $f = 1.495\,\mathrm{kHz}$

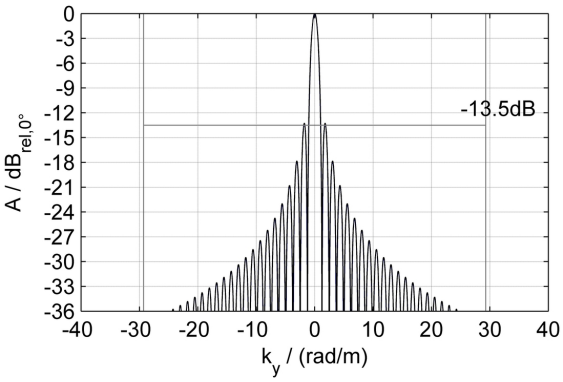

(d) $|D_{w,\mathrm{S}}(k_y,\omega)\cdot H_{\mathrm{Rect}}(k_y,\omega)|$ for $f = 1.6\,\mathrm{kHz}$

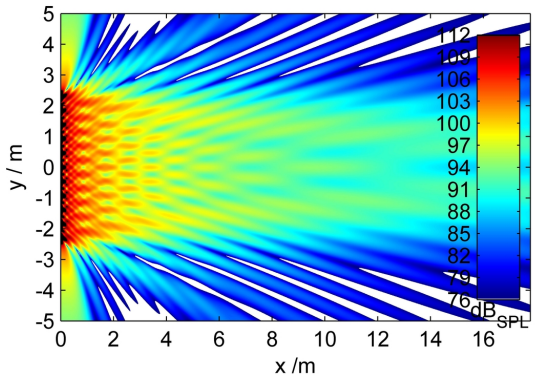

(e) sound field for $f = 1.495\,\mathrm{kHz}$ normalized to
$94\,\mathrm{dB_{SPL}}$ @ $x = 10\,\mathrm{m}, y = 0\,\mathrm{m}$

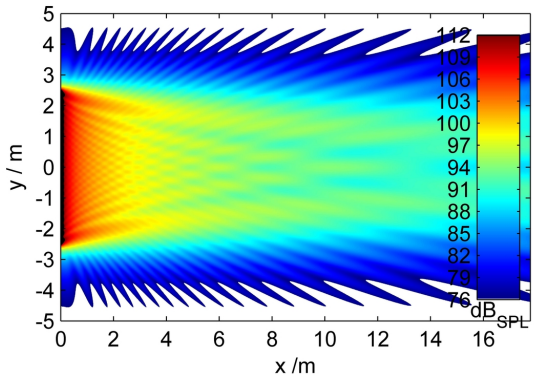

(f) sound field for $f = 1.6\,\mathrm{kHz}$ normalized to
$94\,\mathrm{dB_{SPL}}$ @ $x = 10\,\mathrm{m}, y = 0\,\mathrm{m}$

Fig. 15: Angular spectra and sound fields of a rect windowed line source array, left: with line pistons ($L = 4.9684\,\mathrm{m}$, ARF=0.8436, $N = 11$), right: with line pistons ($L = 5.05\,\mathrm{m}$, ARF=1, $N = 11$)